Tropical Pacific Ocean heat content variations and ENSO persistence barriers

Michael J. McPhaden

Pacific Marine Environmental Laboratory, National Oceanic and Atmospheric Administration, Seattle, Washington, USA

Received 3 January 2003; accepted 12 March 2003; published 9 May 2003.

[1] Data from the tropical Pacific Ocean for the period 1980–2002 are used to examine the persistence of sea surface temperature (SST) and upper ocean heat content variations in relation to El Niño and the Southern Oscillation (ENSO). The present study demonstrates that, unlike for SST, there is no spring persistence barrier when considering upper ocean heat content. Conversely, there is a persistence barrier for heat content in boreal winter related to a seasonal reduction in variance. These results are consistent with ENSO forecast model studies indicating that accurate initialization of upper ocean heat content often reduces the prominence of the spring prediction barrier for SST. They also suggest that initialization of upper ocean heat content variations may lead to seasonally varying enhancements of forecast skill, with the most pronounced enhancements for forecasts starting early and late in the development of ENSO events. *INDEX TERMS:* 4522 Oceanography: Physical: El Niño; 4215 Oceanography: General: Climate and interannual variability (3309); 4504 Oceanography: Physical: Air/sea interactions (0312); 4231 Oceanography: General: Equatorial oceanography. **Citation:** McPhaden, M. J., Tropical Pacific Ocean heat content variations and ENSO persistence barriers, *Geophys. Res. Lett.*, *30*(9), 1480, doi:10.1029/2003GL016872, 2003.

1. Introduction

[2] The El Niño/Southern Oscillation (ENSO) phenomenon is the most pronounced year-to-year fluctuation of the climate system on earth. ENSO originates in the tropical Pacific Ocean and oscillates between warm phases (El Niños) and cold phases (La Niñas) with a periodicity of roughly every three to seven years. ENSO events have significant impacts on global patterns of weather variability, on Pacific marine ecosystems, and on commercial fisheries. For these reasons, considerable effort has been invested in developing ENSO forecast models that can be used to predict conditions in the tropical Pacific several seasons in advance [*Latif et al.*, 1998; *Barnston et al.*, 1999].

[3] A well-known characteristic of ENSO forecasts is that they often show a significant drop off in skill during boreal spring [*Webster and Yang*, 1992]. This so-called "spring barrier" to prediction is paralleled by a reduction in the persistence of observed equatorial Pacific SST anomalies. The earliest explanations for these barriers invoked intrinsic limitations to ENSO predictability as a result of relatively weak coupling between the ocean and atmosphere during boreal spring [e.g., *Zebiak and Cane*, 1987; *Battisti*, 1988]. More recently, it has been argued that SST anomalies in boreal spring are relatively small due to phase locking of the ENSO cycle (or elements of it such as the biennial oscillation) to the annual cycle [*Torrence and Webster*, 1998; *Clarke and van Gorder*, 1999] making it more difficult to detect and forecast these anomalies with accuracy in the face of atmospheric and oceanic noise [*Xue et al.*, 1994; *Chen et al.*, 1995; *Kirtman et al.*, 2002].

[4] *Torrence and Webster* [1998] suggested that this spring barrier to prediction could be bridged in ENSO forecast schemes by taking advantage of ENSO-related persistence in other parts of the climate system. Consistent with this idea, ENSO models often show improvements in forecast skill across the spring barrier when observed variations in upper ocean heat content are included as part of the forecast initialization scheme [*Smith et al.*, 1995; *Xue et al.*, 2000]. This improvement is one manifestation of the principal that ENSO forecasting skill generally increases, especially at longer 6–12 month lead times, by accurately initializing the mean oceanic thermal structure and slow variations in upper ocean heat content associated with low frequency equatorial waves [*Ji and Leetmaa*, 1997; *Latif et al.*, 1998]. These waves adjust the ocean to changes in wind forcing and feedback to the atmosphere indirectly through their influence on ocean mixed layer temperatures [*Battisti*, 1988; *Schopf and Suarez*, 1988]. Statistically, predictability associated with upper ocean heat content derives from the fact that interannual anomalies in heat content (or equivalents such as warm water volume and sea level) near the equator lead those in equatorial SST by several months. This phase relationship is observed both in ocean models used for dynamical forecasting and in observations [*Zebiak and Cane*, 1987; *Zebiak*, 1989; *Balmaseda et al.*, 1995, *Meinen and McPhaden*, 2000; *Xue et al.*, 2000].

[5] *Balmaseda et al.* [1995] found in their coupled ocean-atmosphere forecast model that, unlike for SST, there was a boreal winter rather than a boreal spring barrier to prediction for ENSO time scale upper ocean heat content anomalies. They argued that this offset in phasing for SST and heat content prediction barriers was important in determining the overall predictability of ENSO during the course of a particular event. By analogy with SST, one would expect that there should be an identifiable winter persistence barrier in observed heat content, but one has yet to be described from ocean observations. The purpose of this note therefore is to describe the seasonal persistence of upper ocean heat content anomalies, its underlying dynamics, and its relation to SST variability on ENSO time scales.

2. Data Sets and Data Processing

[6] We use the *Smith* [1995] upper ocean temperature analysis based primarily on ship of opportunity XBT

measurements and TAO/TRITON moored time series measurements [*McPhaden et al.*, 2001]. From this analysis, we compute monthly averages of warm water volume (WWV) between 5°N and 5°S integrated across the Pacific basin including all ocean areas between 80°W and 120°E. The lower boundary for this integration is the depth of the 20°C isotherm, which is located in the middle of the upper thermocline. The 5°N–5°S latitudinal range is chosen to maximize the zonally coherent accumulation and loss of warm water along the equator on ENSO time scales. Other measures of upper ocean heat content could be used (e.g., temperature averaged vertically over the upper 300 m as in *Hasegawa and Hanawa* [2003]), but they all provide essentially the same measure of variability.

[7] The time series of WWV begins in 1980, when sufficient XBT data first became available for reliable basin scale analyses, and runs through December 2002. Monthly anomalies are computed by subtracting out the mean seasonal cycle for the period 1980–2002. We similarly compute NINO 3.4 SST anomalies (5°N–5°S, 120°W–170°W) relative to the 1980–2002, using the *Reynolds and Smith* [1995] SST analysis.

[8] A plot of monthly anomalies in WWV and NINO3.4 SST shows the tendency for NINO3.4 SST to lag WWV by several months (Figure 1). Thus, variations in WWV are valuable precursors to the development of warm and cold ENSO SST anomalies. The basic relationships between these variables, and how they are consistent with the recharge oscillator [*Jin*, 1997] and the delayed oscillator [*Battisti*, 1988; *Schopf and Suarez*, 1988] theories of ENSO, are described in *Meinen and McPhaden* [2000]. In the following section we will explore aspects of how these relationships vary with season.

3. Results

[9] Persistence can be defined in terms of autocorrelation coefficients and the extent to which they remain at significantly high levels for extended lead times. Using correlations >0.7 as a robust measure of significance (the 95% significance level for the null hypothesis is 0.41), SST anomalies starting March–May have the least persistence (correlations falling below 0.7 after only 1–2 months) while those starting in June–August tend to have the greatest persistence (correlations >0.7 for lead times of 7–9 months) (Figure 2a). This seasonality leads to a boreal spring persistence barrier in SST

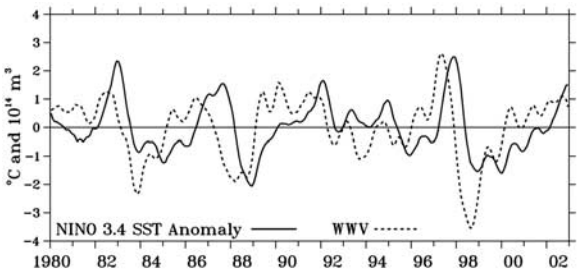

Figure 1. Monthly anomalies of WWV (5°N–5°S, 80°W–120°E above the 20°C isotherm) and NINO3.4 SST (5°N–5°S, 120°W–170°W). Time series have been smoothed with a 5-month running mean filter for display, though all computations are based on unsmoothed monthly anomalies.

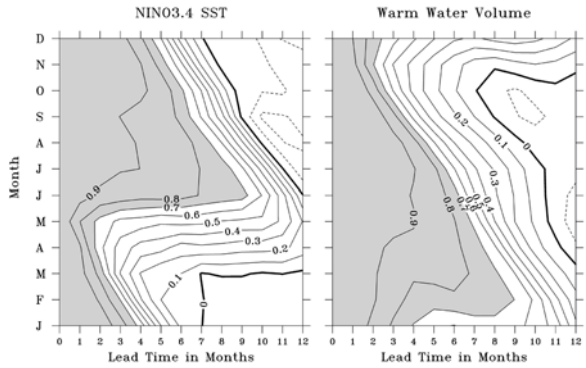

Figure 2. Lag correlation of monthly anomalies in (a) NINO3.4 SST and (b) WWV as a function of start month and lead-time. Correlations above 0.41 are significant at the 95% level of confidence assuming each of the 23 years of data is independent (supported by the low correlations at 12 month leads). Correlations greater than 0.7 are shaded.

in which correlations drop to insignificant levels during the spring season at either short lead-times beginning early in the calendar year or longer lead times beginning in the previous boreal summer or autumn.

[10] In contrast, WWV does not show a spring persistence barrier. In fact, highly persistent WWV anomalies occur beginning in late boreal winter and early spring when SST persistence is weakest. Correlations for WWV are >0.7 at lead times of 7–9 months for anomalies starting in February through May (Figure 2b). Conversely, for WWV anomalies starting in September–November, correlations fall below 0.7 by early boreal winter after only about 2–3 months. This indicates that WWV anomalies present near the end of the calendar year will not persist past the following winter season whereas anomalies present in late boreal winter and spring will persist for 2–3 seasons.

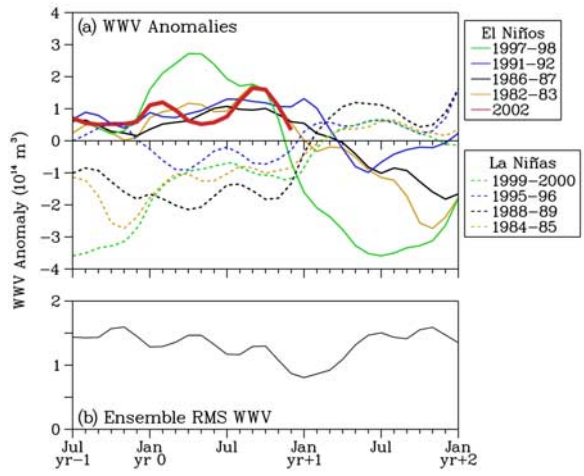

Figure 3. (a) Warm water volume anomalies for El Niños (solid lines) and La Niñas (dashed lines) since 1980. (b) Ensemble root mean square (rms) WWV anomaly. Time axis starts in July the year before the warm or cold event (Jul, Yr − 1) and continues through January the year after the end of the event (Jan, Yr + 2). For example, the time axis for the 1997–98 El Niño is July 1996 to January 1999.

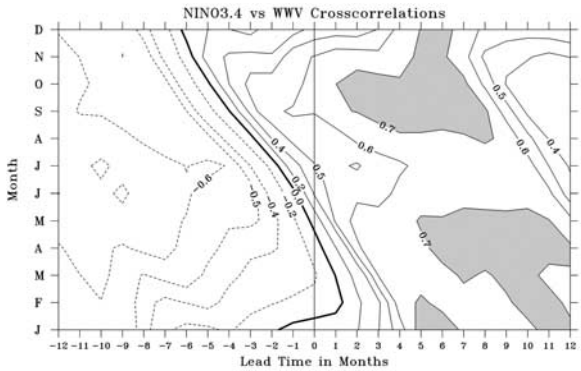

Figure 4. Crosscorrelation between monthly WWV and NINO3.4 SST anomalies as a function of start month and lead-time. Positive (negative) leads imply WWV leads (lags) SST. Correlations above 0.41 are significant at the 95% level of confidence assuming each of the 23 years of data is independent. Correlations greater than 0.7 are shaded.

[11] The persistence of WWV anomalies beginning early in the calendar year through boreal autumn is consistent with the recharge oscillator theory of ENSO which predicts that the time prior to the development of largest magnitude SST anomalies is when WWV anomalies reach their greatest magnitude. The excess of equatorial WWV during the growth phase of an El Niño for example results primarily from anomalous heat transports towards the equator from higher latitudes prior to and during the onset of the event. However, as El Niño approaches maturity, excess warm water volume is purged to higher latitudes and WWV decreases sharply near the equator (Figure 3a) [see also *Meinen and McPhaden*, 2000]. Thus, in boreal winter near the height of El Niño, WWV anomalies are reduced to relatively small values.

[12] The same sequence of events, but with opposite sign, operates during the cold phase of the ENSO cycle (Figure 3a). Thus, for the boreal winter season during which El Niño or La Niña events mature, WWV anomaly variance tends to be small (Figure 3b). By analogy with the spring-time barrier in SST persistence, phase locking of WWV variations to the seasonal cycle leads to low signal variance during the boreal winter of ENSO years and therefore increased sensitivity to noise contamination in the computation of correlation coefficients at that time [*Xue et al.*, 1994]. As a consequence, a WWV persistence barrier develops in boreal winter, consistent with the modeling results of *Balmaseda et al.* [1995].

[13] The above results also indicate how forecast model initialization schemes that include upper ocean heat content (or equivalently sea level) can bridge the spring barrier to SST prediction. For the boreal winter and spring season prior to the mature phase of ENSO events, anomalous WWV is a much better predictor of NINO3.4 SST than NINO3.4 is itself at lead times longer than about three months. Although the in-phase correlation of these two quantities is near zero during the first six months of the calendar year, correlations above 0.7 are found for February–April anomalies in WWV leading NINO3.4 SST by 9–10 months (Figure 4). Persisted February–April SST anomalies would show no skill at these lead times.

[14] The pattern of SST and wind stress anomalies in December–February based on a typical 1×10^{14} m^3 WWV anomaly 10 months earlier (February–April) during the onset phase of El Niño is shown in Figure 5. This pattern was determined by regressing December–February SST and wind stress components against the previous February–April WWV values, then computing the magnitude of predicted anomalies based on the regression coefficients. The pattern is characteristic of mature phase El Niño conditions [*Rasmusson and Carpenter*, 1982; *Harrison and Larkin*, 1998] and is consistent with the dominant empirical orthogonal eigenfunction pattern for ENSO time scale SST and wind anomalies [*Xue et al.*, 2000]. Warm SST anomalies (maximum of 1.2°C) are evident along the equator in the central and eastern Pacific and along the west coasts of the Americas. Surrounding these warm anomalies are cold SSTs to the west, north, and south. Westerly wind

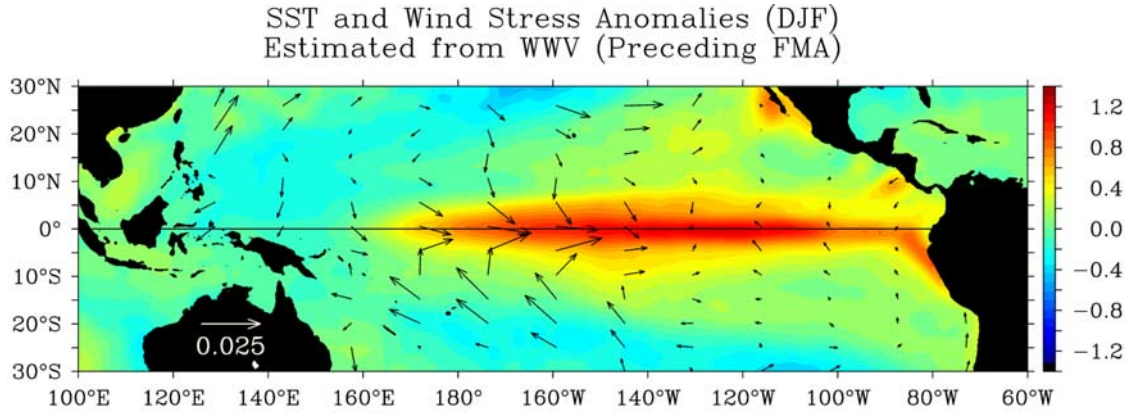

Figure 5. Regression estimates of anomalous surface wind stress (in N m^{-2}) and SST (in °C) for December–February based on warm water volume estimates during the preceding February–April. Scale for wind anomalies is overplotted on Australia, scale for SST anomalies is to the right of the plot. Stress is computed from the Florida State University (FSU) wind pseudostress [*Stricherz et al.*, 1997] using an air density of 1.2 kg m^{-3} and a constant drag coefficient of 1.4×10^{-3}. Stress anomalies are computed relative to the mean seasonal cycle over 1980–2002.

stress anomalies (maximum of 0.04 N m^{-2}) are apparent in the western and central equatorial Pacific while easterly wind stress anomalies are evident in the eastern equatorial Pacific, the far western equatorial Pacific, and the higher latitudes of the North and South Pacific. The pattern in Figure 5 would be of opposite sign for a February–April WWV anomaly of -1×10^{14} m^3, characteristic of La Niña conditions.

4. Discussion and Conclusion

[15] Results of the previous section indicate that persistence in upper ocean heat content anomalies is strongest in the early part of the calendar year coincident with the onset phase of ENSO events when SST anomalies are weak. This helps to explain why accurate initialization of upper ocean heat content in ENSO forecast models often reduces the prominence of the spring SST prediction barrier [e.g., *Smith et al.*, 1995; *Xue et al.*, 2000]. *Chen et al.* [1995] also demonstrated that an improved initialization procedure developed to reduce noise in the wind stress field effectively eliminated the spring barrier to prediction in the *Zebiak and Cane* [1987] intermediate coupled ocean-atmosphere ENSO forecast model. Part of the improvement in forecast skill in their study came from reduced errors in SST initial conditions. However, initialization of upper ocean heat content in their model was via the time history of wind forcing, so that improving the initialization for winds also improved the initialization for upper ocean heat content.

[16] These results indicate that potential contribution to predictive skill provided by subsurface ocean temperature information may vary over the course of an ENSO event. For example, upper ocean heat content variations may affect predictability most significantly at 6–12 month lead times early and late in the development of warm and cold events when large scale SST and wind anomalies are weak. Conversely, heat content variations may be less of a constraint at these lead times for forecasts starting late in the calendar year as events approach maturity. Consistent with these results, evidence for seasonality in the effectiveness of upper ocean heat content as a constraint in ENSO forecast model initialization has be found in *Balmaseda et al.* [1995], *Smith et al.* [1995] and *Xue et al.* [2000]. The present analysis may therefore be of value in interpreting the effectiveness of subsurface temperature data initialization in future ENSO model forecast studies and in designing improved ENSO forecast initialization methodologies.

[17] **Acknowledgments.** The author would like to thank Magdelena Balmaseda, Ben Kirtman, Yan Xue, Tony Barnston, and Tony Busalacchi for helpful comments and suggestions on earlier versions of this manuscript. The analysis was supported by NOAA's Office of Oceanic and Atmospheric Research and by the Joint Institute for the Study of the Atmopshere and Ocean (JISAO) at the University of Washington under NOAA Cooperative Agreement NA17RJ11232. PMEL publication number 2548 and JISAO publication number 974.

References

Balmaseda, M. A., M. K. Davey, and D. L. T. Anderson, Decadal and seasonal dependence of ENSO prediction skill, *J. Clim.*, *8*, 2705–2715, 1995.

Barnston, A. G., Y. He, and M. H. Glantz, Predictive skill of statistical and dynamical climate models in SST forecasts during the 1997–98 El Niño episode and the 1998 La Niña onset, *Bull. Am. Meteorol. Soc.*, *80*, 217–244, 1999.

Battisti, D. S., Dynamics and thermodynamics of a warming event in a coupled atmosphere-ocean model, *J. Atmos. Sci.*, *45*, 2889–2919, 1988.

Chen, D., S. E. Zebiak, A. J. Busalacchi, and M. A. Cane, An improved procedure for El Niño forecasting, *Science*, *269*, 1699–1702, 1995.

Clarke, A. J., and S. van Gorder, The connection between the boreal spring Southern Oscillation persistence barrier and biennial variability, *J. Clim.*, *12*, 610–620, 1999.

Harrison, D. E., and N. K. Larkin, El Niño-Southern Oscillation sea surface temperature and wind anomalies, *Rev. Geophys.*, *36*, 353–399, 1998.

Hasegawa, T., and K. Hanawa, Heat content related to ENSO variability in the Pacific, *J. Phys. Oceanogr.*, *33*, 407–421, 2003.

Ji, M., and A. Leetmaa, Impact of data assimilation on ocean initialization and El Niño prediction, *Mon. Weather Rev.*, *125*, 742–753, 1997.

Jin, F. F., An equatorial recharge paradigm for ENSO. part I: Conceptual model, *J. Atmos. Sci.*, *54*, 811–829, 1997.

Kirtman, B. P., J. Shukla, M. Balmaseda, N. Graham, C. Penland, Y. Xue, and S. Zebiak, Current status of ENSO forecast skill: A report to the Climate Variability and Predictability (CLIVAR) Numerical Experimentation Group (NEG), CLIVAR Working Group on Seasonal to Interannual Prediction, Clim. Variability and Predictability, Southampton Oceanogr. Cent., Southampton, UK, 2002. (Available at http://www. clivar.org/publications/wg_reports/wgsip/nino3/report.htm.).

Latif, M., D. Anderson, T. Barnett, M. Cane, R. Kleeman, A. Leetmaa, J. O'Brien, A. Rosati, and E. Schneider, A review of the predictability and prediction of ENSO, *J. Geophys. Res.*, *103*, 14,375–14,393, 1998.

McPhaden, M. J., T. Delcroix, K. Hanawa, Y. Kuroda, G. Meyers, J. Picaut, and M. Swenson, The El Niño/Southern Oscillation (ENSO) observing system, in *Observing the Ocean in the 21st Century*, pp. 231–246, Aust. Bur. of Meteorol., Melbourne, 2001.

Meinen, C. S., and M. J. McPhaden, Observations of warm water volume changes in the equatorial Pacific and their relationship to El Niño and La Niña, *J. Clim.*, *13*, 3551–3559, 2000.

Rasmusson, E. M., and T. H. Carpenter, Variations in tropical sea surface temperature and surface wind fields associated with the Southern Oscillation/El Niño, *Mon. Weather Rev.*, *110*, 354–384, 1982.

Reynolds, R. W., and T. M. Smith, A high resolution global sea surface temperature climatology, *J. Clim.*, *8*, 1572–1583, 1995.

Schopf, P. S., and M. J. Suarez, Vacillations in a coupled ocean-atmosphere model, *J. Atmos. Sci.*, *45*, 549–566, 1988.

Smith, N. R., An improved system for tropical ocean sub-surface temperature analyses, *J. Atmos. Oceanic Technol.*, *12*, 850–870, 1995.

Smith, T., A. G. Barnston, M. Ji, and M. Chelliah, The impact of Pacific Ocean subsurface data on operational prediction of tropical Pacific SST at the NCEP, *Weather Forecasting*, *10*, 708–714, 1995.

Stricherz, J. N., D. M. Legler, and J. J. O'Brien, *TOGA Pseudo-Stress Atlas, 1985–94*, vol. II, Pacific Ocean, Fla. State Univ., Tallahassee, 155 pp., 1997.

Torrence, C., and P. J. Webster, The annual cycle of persistence in the El Niño/Southern Oscillation, *Q. J. R. Meteorol. Soc.*, *124*, 1985–2004, 1998.

Webster, P. J., and S. Yang, Monsoon and ENSO: Selectively interactive systems, *Q. J. R. Meteorol. Soc.*, *118*, 825–877, 1992.

Xue, Y., M. A. Cane, S. E. Zebiak, and M. B. Blumenthal, On the prediction of ENSO: A study with a low-order Markov model, *Tellus, Ser. A*, *46*, 512–528, 1994.

Xue, Y., A. Leetmaa, and M. Ji, ENSO prediction with Markov models: The impact of sea level, *J. Clim.*, *13*, 849–871, 2000.

Zebiak, S., Ocean heat content variability and ENSO cycles, *J. Phys. Oceanogr.*, *19*, 475–485, 1989.

Zebiak, S. E., and M. A. Cane, A model of El Niño-Southern Oscillation, *Mon. Weather Rev.*, *115*, 2262–2278, 1987.

M. J. McPhaden, NOAA/Pacific Marine Environmental Laboratory, Seattle, WA 98115, USA. (mcphaden@pmel.noaa.gov)